



1 **One-Year Simulation of Ozone and Particulate Matter in China**
2 **Using WRF/CMAQ Modeling System**

3
4 Jianlin Hu¹, Jianjun Chen^{2,1}, Qi Ying^{3,1,*}, Hongliang Zhang^{4,1,*}

5
6 ¹Jiangsu Key Laboratory of Atmospheric Environment Monitoring and Pollution Control, Jiang-
7 su Engineering Technology Research Center of Environmental Cleaning Materials, Collaborative
8 Innovation Center of Atmospheric Environment and Equipment Technology, School of Envi-
9 ronmental Science and Engineering, Nanjing University of Information Science & Technology,
10 219 Ningliu Road, Nanjing 210044, China

11 ²Air Quality Planning and Science Division, California Air Resources Board, 1001 I Street, Sac-
12 ramento, CA 95814, USA

13 ³Zachry Department of Civil Engineering, Texas A&M University, College Station, TX 77843,
14 USA

15 ⁴Department of Civil and Environmental Engineering, Louisiana State University, Baton Rouge
16 LA 70803, USA

17
18 *Corresponding authors:

19 Qi Ying, Email: qying@civil.tamu.edu. Phone: +1-979-845-9709.

20 Hongliang Zhang, Email: hlzhang@lsu.edu. Phone: +1-225-578-0140.

21 **Abstract**

22 China has been experiencing severe air pollution in recent decades. Although ambient air quality
23 monitoring network for criteria pollutants has been constructed in over 100 cities since 2013 in
24 China, the temporal and spatial characteristics of some important pollutants, such as particulate
25 matter (PM) components, remain unknown, limiting further studies investigating potential air
26 pollution control strategies to improve air quality and associating human health outcomes with
27 air pollution exposure. In this study, a yearlong (2013) air quality simulation using the Weather
28 Research & Forecasting model (WRF) and the Community Multi-scale Air Quality model
29 (CMAQ) was conducted to provide detailed temporal and spatial information of ozone (O₃),
30 PM_{2.5} total and chemical components. Multi-resolution Emission Inventory for China (MEIC)
31 was used for anthropogenic emissions and observation data obtained from the national air quality
32 monitoring network were collected to validate model performance. The model successfully re-
33 produces the O₃ and PM_{2.5} concentrations at most cities for most months, with model perfor-
34 mance statistics meeting the performance criteria. However, over-prediction of O₃ generally oc-
35 curs at low concentration range while under-prediction of PM_{2.5} happens at low concentration
36 range in summer. Spatially, the model has better performance in Southern China than in North-
37 ern, Central and Sichuan basin. Strong seasonal variations of PM_{2.5} exist and wind speed and di-
38 rection play important roles in high PM_{2.5} events. Secondary components have more boarder dis-
39 tribution than primary components. Sulfate (SO₄²⁻), nitrate (NO₃⁻), ammonium (NH₄⁺), and pri-
40 mary organic aerosol (POA) are the most important PM_{2.5} components. All components have the
41 highest concentrations in winter except secondary organic aerosol (SOA). This study proves the
42 ability of CMAQ model in reproducing severe air pollution in China, identifies the directions
43 where improvements are needed, and provides information for human exposure to multiple pol-
44 lutants for assessing health effects.

45 **Keywords:** Ozone, Particulate matter, WRF, CMAQ, MEIC, China

46



47 1. Introduction

48 Atmospheric pollutants have adverse effects on human health and ecosystems and are associated
49 with climate change (Menon et al., 2008; Poschl, 2005; Pui et al., 2014). Developing countries
50 usually experience severely high concentrations of air pollutants due to fast growth of population,
51 industrialization, transportation and urbanization without prompt emission controls. As one of
52 such countries, China started to publish real time concentration data of six criteria pollutants
53 from the ambient air quality monitoring networks after multiple severe pollution events across
54 the country (Sun et al., 2014; Tao et al., 2014b; Wang et al., 2014a; Zheng et al., 2015).

55 More than 1000 observation sites have been set up in more than 100 major cities in the country
56 to routinely monitor hourly concentrations of six criteria pollutants, i.e., O₃, CO, NO₂, SO₂,
57 PM_{2.5} (PM—particulate matter), and PM₁₀, and to inform the public on air quality status using
58 the air quality index (AQI). Analysis of the observation provided a general understanding of the
59 spatial and temporal variation of the levels of air pollution (Hu et al., 2014a; Wang et al., 2014c),
60 the roles of meteorology in air pollution (Zhang et al., 2015b), and the construction of AQI based
61 on multiple pollutants to better inform the public about the severity of air pollution (Hu et al.,
62 2015b). However, the monitoring system only considers criteria pollutants and the key species
63 such as the volatile organic compounds (VOCs) and the chemical composition of PM that are
64 needed to understand the causes of air pollution and form cost-effective emissions controls are
65 not measured routinely. Monitoring networks focusing on the chemical composition of gaseous
66 and particulate air pollutants, such as the Photochemical Assessment Monitoring Stations
67 (PAMS) and the Chemical Speciation Network (CNS) in the United States, have not been estab-
68 lished in China. Lacking of detailed chemical composition information limits our capability to
69 understand the formation mechanisms of O₃ and PM, quantify the contributions of different
70 sources, and design effective control strategies. In addition, the observation sites are mostly in
71 highly developed urban areas but are very sparse in other suburban and rural regions which also
72 have large population and experience high concentrations of certain pollutants, such as O₃. Insuf-
73 ficient spatial coverage in the monitoring system limits the completeness of public air pollution
74 risk assessment for the entire country.

75 Chemical transport models (CTMs) are often used to reproduce past pollution events, test newly
76 discovered atmospheric mechanisms, predict future air quality, and provide high temporal and
77 spatial resolution data for epidemiological studies. Several modeling studies have been reported
78 to analyze the severe air pollution events in January 2013. For example, the Community Mul-
79 tiscalaire Air Quality (CMAQ) model was updated with heterogeneous chemistry to study the for-
80 mation of secondary inorganic aerosol in North China (Zheng et al., 2015). The CMAQ model
81 was also applied to identify the contributions of both source regions and sectors to PM_{2.5} in
82 Southern Hebei during the 2013 severe haze episode with a brute force method (Wang et al.,
83 2014b). It was found that industrial and domestic activities were the most significant local sec-
84 tors while Northern Hebei province, Beijing-Tianjin city cluster, and Henan province were the
85 major regional contributors. Using the two-way coupled Weather Research and Forecasting
86 (WRF)/CMAQ system, Wang et al. (2014b) simulated the impacts of aerosol–meteorology inter-
87 actions on the PM pollution during January 2013. They argued that enhanced planetary boundary
88 layer (PBL) stability suppressed the dispersion of air pollutants, and resulted in higher PM_{2.5}
89 concentrations. Similar results were also reported by Zhang et al. (2015a) with the Weather Re-
90 search and Forecasting/Chemistry (WRF/Chem) model. Using the Comprehensive Air Quality



91 Model with extensions (CAMx) and the Particulate Source Apportionment Technology (PSAT),
92 Li et al. (2015b) determined the contributions of 7 emission categories and 11 source regions to
93 regional air pollution in China and suggested a strong need for regional joint emission control
94 efforts in Beijing. More recently, Hu et al. (2015a) used a tracer based technique in a source-
95 oriented CMAQ to determine source sector/region contributions to primary PM in different sea-
96 sons in 2012-2013. It was found that residential and industrial emissions from local area and the
97 neighboring Hebei province contribute to high primary PM events in Beijing.

98 All above modeling studies except Hu et al. (2015a) were focused on the formation and source
99 apportionment of airborne PM during the severe pollution episode of January 2013 in northern
100 China. Although additional PM formation pathways and/or emission adjustments were imple-
101 mented and tuned to better predict this extreme episode, model predictions were only evaluated
102 against a small number of measurements in and near Beijing for a relatively short period of time.
103 Extensive model performance evaluation of O₃ and PM is urgently needed to build the confi-
104 dence in the emission inventory, the predicted meteorological fields as well as the capability of
105 the model in predicting regional O₃ and PM under a wide range of topographical, meteorological
106 and emission conditions so that further modeling studies of pollutant formation mechanisms,
107 emission control strategies, and human exposure and health risk assessment are based on a solid
108 foundation.

109 In this study, a yearlong (2013) air quality simulation using a WRF/CMAQ system was conduct-
110 ed to provide detailed temporal and spatial distribution of O₃ and PM concentrations as well as
111 PM_{2.5} chemical composition in China. The publicly available observation data obtained from a
112 total of 422 air monitoring sites in 60 major cities in China were used to provide a thorough
113 evaluation of the model performance in the entire year. The modeled spatial and temporal con-
114 centrations of O₃ and PM_{2.5} from this study will be used in subsequent studies to investigate the
115 interaction between O₃ and PM pollution during high pollution events, the formation mechanism
116 of secondary inorganic and organic aerosols and the population exposure and health risk.

117 **2. Method**

118 **2.1 Model description**

119 The CMAQ model applied in this study is based on CMAQ v5.0.1. Changes were made to the
120 original CMAQ to improve the capability of the model in predicting secondary inorganic and
121 organic aerosol, including 1) a modified SARPC-11 gas phase photochemical mechanism to pro-
122 vide more detailed treatment of isoprene oxidation chemistry (Ying et al., 2015), 2) pathways of
123 secondary organic aerosol (SOA) formation from surface controlled reactive uptake of dicarbon-
124 yls, isoprene epoxydiol (IEPOX) and methacrylic acid epoxide (MAE) (Li et al., 2015a; Ying et
125 al., 2015), 3) vapor wall-loss corrected SOA yields (Zhang et al., 2014), and 4) heterogeneous
126 reactions of NO₂ and SO₂ on particle surface to form secondary nitrate and sulfate (Ying et al.,
127 2014a). More details of these changes can be found in the cited references and the references
128 therein, thus only a short summary of the changes are provided below.

129 The isoprene mechanism in the original SARPC-11 with standard lumping (Carter and Heo,
130 2012) was replaced by the detailed isoprene oxidation chemistry as used by Lin et al. (2013) to
131 predict the formation of IEPOX and MAE in the gas phase. A precursor tracking scheme was



132 implemented in the modified SAPRC-11 to track the glyoxal (GLY) and methylglyoxal (MGLY)
133 formation from multiple biogenic and anthropogenic precursors. The surface controlled reactive
134 uptake of SOA precursors is considered non-reversible, with constant uptake coefficients for
135 GLY and MGLY as used by Fu et al. (2008) and an acidity dependent uptake coefficient for IE-
136 POX and MAE as described by Li et al. (2015a). The original SOA yields for toluene and xylene
137 under high NO_x concentrations based on Ng et al. (2007) were replaced with the higher toluene
138 yield reported by Hildebrandt et al. (2009). This update has been applied by Ying et al. (2014a)
139 to study SOA formation in Mexico City. All SOA yields were then corrected by the average bias
140 due to wall loss as reported in Table 1 of Zhang et al. (2014). A modeling study of SOA for-
141 mation in Eastern US reported by Ying et al. (2015) shows that negative bias in predicted organ-
142 ic carbon (OC) concentrations reported in previous studies have been significantly reduced.
143 Formation of sulfate and nitrate due to heterogeneous reactions on particle surface is also mod-
144 eled as a reactive uptake process. The reactive surface uptake coefficients of SO₂ and NO₂ on
145 particle surface were taken from Ying et al. (2014a) and Zheng et al. (2015), respectively.

146 2.2 Model application

147 The updated CMAQ model was applied to simulate O₃ and particulate air pollution using a 36-
148 km horizontal resolution domain that covers China and surrounding countries in East Asia (Fig-
149 ure 1). The meteorological inputs were generated using WRF v3.6.1 with initial and boundary
150 conditions from the NCEP FNL Operational Model Global Tropospheric Analyses dataset. De-
151 tailed WRF model configurations have been described by Zhang et al. (2012).

152 Multi-resolution Emission Inventory for China (MEIC) (0.25°×0.25°) developed by Tsinghua
153 University (<http://www.meicmodel.org>) was used for the monthly anthropogenic emissions from
154 China. MEIC (V1.0) is the new version of emission inventory in China including improvements
155 such as a unit-based emission inventory for power plants (Wang et al., 2012) and cement plants
156 (Lei et al., 2011), a high-resolution county-level vehicle emission inventory (Zheng et al., 2014),
157 and a non-methane VOC mapping approach for different chemical mechanisms (Li et al., 2014b).
158 MEIC provides speciated VOC emissions for the SAPRC-07 mechanism with standard lumping
159 (Carter, 2010). As the definitions of explicit and lumped primary VOCs have not changed from
160 SAPRC-07 to SAPRC-11, these VOC emissions were directly used to drive SAPRC-11. Total
161 PM_{2.5} mass emissions and emissions of primary organic carbon (POC) and elemental carbon (EC)
162 were also provided by MEIC directly. Emissions of trace metals needed by the version 6 of the
163 aerosol module in CMAQ (AERO6) were generated using averaged speciation profiles adapted
164 from the U.S. Environmental Protection Agency (EPA) SPECIATE database for each MEIC
165 source category. Emissions from other countries and regions rather than China in the domain
166 were filled with data generated from the gridded 0.25°×0.25° resolution Regional Emission in-
167 ventory in ASia version 2 (REAS2) (Kurokawa et al., 2013). Details of the REAS2 emission
168 processing are described by Qiao et al. (2015). Detailed information about spatial and temporal
169 allocation can also be found in the papers cited above.

170 Biogenic emissions were generated using the Model for Emissions of Gases and Aerosols from
171 Nature (MEGAN) v2.1. The leaf area index (LAI) was based on the 8-day Moderate Resolution
172 Imaging Spectroradiometer (MODIS) LAI product (MOD15A2) and the plant function types
173 (PFTs) were based on the PFT files used in the Global Community Land Model (CLM 3.0). For
174 more details of the biogenic emission processing, the readers are referred to Qiao et al. (2015).



175 Open biomass burning emissions were generated from the Fire INventory from NCAR (FINN),
176 which is based on satellite observations (Wiedinmyer et al., 2011). Dust and sea salt emissions
177 were generated in line during the CMAQ simulations. In this updated CMAQ model, dust emis-
178 sion module was updated to be compatible with the 20-category MODIS land use data (Hu et al.,
179 2015a). Initial and boundary conditions were based on the default vertical distributions of con-
180 centrations that represent clean continental conditions as provided by the CMAQ model. The im-
181 pact of initial conditions was minimal as the results of the first five days of the simulation were
182 excluded in the analyses.

183 3. Results

184 3.1 Meteorology validation

185 Meteorological factors are closely related to transport, transformation, and deposition of air pol-
186 lutants (Hu et al., 2014b; Jacob and Winner, 2009; Tao et al., 2014a; Zhang et al., 2015b). Alt-
187 hough the WRF model has been widely used to provide meteorological inputs for CTMs, the per-
188 formance varies when applying to different domains, episodes, and with different model settings.
189 Thus, the validation of model performance on meteorological conditions is important in assuring
190 the accuracy of air quality predictions. Observation data from the National Climate Data Center
191 (NCDC) was used to validate the model predictions of temperature (T2) and relative humidity
192 (RH) at 2m above surface, and wind speed (WS) and wind direction (WD) at 10m above surface.
193 Within the domain, there are ~1200 stations shown as purple dots in Figure 1. Model perfor-
194 mance statistics of mean observation (OBS), mean prediction (PRE), mean bias (MB), gross er-
195 ror (GE) and root mean square error (RMSE) based on the observations and WRF predictions at
196 the grid cells where the stations are located are shown in Table 1. The table also shows the
197 benchmarks suggested by Emery et al. (2012) for the MM5 model in the East US with 4-12km
198 grid resolution.

199 The WRF model predicts slightly higher T2 in winter and lower T2 in other seasons than the ob-
200 servations. The MB values for June, July, and September to December are within the benchmark,
201 but the GE values of T2 are generally larger than the benchmark. The GE values of WS meet the
202 benchmark in all months, but WS is over-predicted, as indicated by the positive MB values. The
203 MB values meet the benchmark in January, June and August, and RMSE values are within the
204 benchmark in June, July, and August. MB values of WD are within the benchmark of ± 10 degree
205 for four months. February, November, and December are the months with largest MB values. All
206 GE values of WD are about 50% larger than the benchmark. RH is generally under-predicted ex-
207 cept for July and August. The performance in this study is comparable to other studies using
208 WRF in China (Hu et al., 2015a; Wang et al., 2010; Wang et al., 2014b; Ying et al., 2014b;
209 Zhang et al., 2012), despite the differences in model, resolution, and study region in different
210 studies. Generally, the WRF model has acceptable performance on meteorological parameters. It
211 should be noted that there is a study showing better WRF performance (Zhao et al., 2013a).
212 However, it is difficult to compare since different model settings, simulation episodes, number of
213 observation stations were used.



214 3.2 Model performance of O₃ and PM_{2.5}

215 Hourly observations of air pollutants from March to December 2013 were obtained from the
216 publishing website of China National Environmental Monitoring Center
217 (<http://113.108.142.147:20035/emcpublish/>). A total of 422 stations in 60 cities (see Figure 1 for
218 the location of the cities) including the capital cities of all 31 provinces were obtained. Pollutants
219 concentrations in difference regions of China exhibit large variations due to diverse climates, to-
220 pography, and emission sources. Aiming to identify the model strength and weakness in differ-
221 ence regions of China, model performance was evaluated separately for different regions. The
222 regions and names of these cities are listed in Table 2. Automated quality control measures were
223 taken to remove data points with observed O₃ concentrations greater than 250 ppb, PM_{2.5} con-
224 centrations greater than 1500 µg m⁻³, and points with standard deviation less than 5 ppb or 5 µg
225 m⁻³ in 24 hours.

226 3.2.1 O₃ model performance

227 Table 3 shows the model performance statistics of gaseous pollutants (1h peak O₃ (O₃-1h), 8h
228 peak O₃ (O₃-8h), and hourly CO, NO₂, and SO₂) PM_{2.5}, and PM₁₀. Mean observations, mean pre-
229 dictions, mean fractional bias (MFB), mean fractional error (MFE), mean normalized bias (MNB)
230 and mean normalized error (MNE) of hourly concentrations are calculated for each month from
231 March to December 2013. Only O₃-1h or O₃-8h concentrations greater than 30 ppb were includ-
232 ed in the analysis. A cutoff concentration of 40 or 60 ppb is suggested by the U.S. EPA (EPA,
233 2005). A lower cutoff of 30 ppb is chosen in this study considering the monitoring sites are all
234 located in urban areas and higher O₃ concentrations generally occurs in downwind of urban areas.
235 The overall model performance on O₃-1h and O₃-8h meets the model performance criteria sug-
236 gested by U.S. EPA (2005) in all months, except in March and April for O₃-1h and June for O₃-
237 8h. MNE of O₃-1h in June and July slightly exceeds the criteria, although MNB meets the crite-
238 ria. MNB of O₃-8h in May exceeds the criteria, but MNE meets the criteria. The relatively small
239 MNB/MNE and MFB/MFE in most of months indicate that O₃-1h and O₃-8h are well captured.

240 Model performance of O₃-1h and O₃-8h in different regions is illustrated in Table 4. Model per-
241 formance meets the criteria in four regions, i.e., North China Plain (NCP), Yangtze River Delta
242 (YRD), Pearl River Delta (PRD), and Northeast (NE). Relatively poor performance is identified
243 in the Sichuan Basin (SCB), Central (CEN), and Northwest (NW) regions. O₃-1h and O₃-8h con-
244 centrations are slightly under-predicted in YRD and PRD, but over-predicted in all other regions.
245 Model performance in regions other than NCP and YRD should be interpreted with care due to
246 limited number of cities to sufficiently represent the entire region.

247 Figure 2 compares the predicted monthly averaged diurnal variations of O₃ concentrations with
248 observations for all the 60 cities. For a city with multiple stations, observations and predictions
249 are matched at individual station level and the averaged observations and predictions are used to
250 represent the concentrations for the city. Some cities, such as Beijing, exhibit substantial diurnal
251 variations, especially in summer; and others, such as Lasa, exhibit small diurnal variations.
252 Overall, the model successfully reproduces the monthly average diurnal variation in most cities,
253 even though model performance among cities in the same region can be quite different. For ex-
254 ample, in NE, the monthly averaged predictions agree well with observations in Shenyang and
255 Changchun but are higher in Dalian, a coastal city, in summer months. In NCP, the model well



256 predicts O_3 concentrations with slight over-prediction at a few cities, especially in the summer
257 months, which agrees with the better hourly O_3 model performance shown in Tables 3 and 4. In
258 YRD, the monthly diurnal variations of O_3 are also well predicted. Obvious under-prediction of
259 summer peak O_3 at Zhoushan and Wenzhou are likely caused by underestimation of emissions in
260 these port cities, although uncertainty in meteorology might also play a role. At PRD, O_3 is
261 slightly underestimated in Guangzhou and Shenzhen for summer and fall months but well esti-
262 mated in Zhuhai. In all three cities in the PRD region, O_3 concentrations are higher in the spring
263 and fall months, and the model correctly captures this trend. In SCB, the model correctly predicts
264 the higher spring O_3 concentrations in Chengdu but over-predicts spring O_3 concentrations in
265 Chongqing. Summer O_3 concentrations are well predicted at both cities. For CEN, O_3 predictions
266 are higher than observations in Zhengzhou and Hefei, but agree well with observations in other
267 cities. In NW, the observed O_3 concentrations are much lower and are generally over-predicted
268 all year except for Xi'an and Wulumuqi with good performance in summer.

269 Figure 3 shows the comparison of predicted and observed monthly averaged O_3 -1h and O_3 -8h
270 concentrations at typical cities of major regions in China: Beijing for NCP, Shanghai for YRD,
271 Guangzhou for PRD, Xi'an for NW, Shenyang for NE, and Chongqing for SCB. In Beijing, the
272 monthly variations of both O_3 -1h and O_3 -8h, low in winter months and high in summer months,
273 are well captured by model. The model slightly over-predicts O_3 concentrations from June to
274 December except for August. In Shanghai, both O_3 -1h and O_3 -8h are underestimated by 5-10 ppb,
275 but all observations are within the range of concentrations in the 3×3 grid cells surrounding the
276 city center of Shanghai. In Guangzhou, O_3 concentrations vary slightly over months. O_3 -1h is
277 under-predicted especially in summer and fall months. O_3 -8h predictions are closer to the obser-
278 vations. In Xi'an, the model well predicts the O_3 -1h and O_3 -8h concentrations in July, August,
279 and September while over-predicts all other months by up to 20 ppb. In Shenyang, the trend of
280 O_3 -1h and O_3 -8h are well reproduced with less than 5ppb differences for all the months. In
281 Chongqing, over-prediction occurs in spring, fall, and winter while under-prediction occurs in
282 summer.

283 3.2.2 $PM_{2.5}$ model performance

284 $PM_{2.5}$ model performance in different months and regions are also illustrated in Table 3 and Ta-
285 ble 4, respectively. The model performance statistics of MFB and MFE of hourly $PM_{2.5}$ concen-
286 trations meet the US EPA criteria in all months. Negative MFB is found in all months, indicating
287 the model under-predicts the $PM_{2.5}$ concentrations. Model performance is better in March, Sep-
288 tember, November and December, with MFB less than 0.3. The bias is relatively larger in April,
289 May, June, July and October, with MFB over 0.4. PM_{10} is largely underestimated and is very
290 likely to due to underestimation of dust emissions from both natural sources as well as human
291 activities.

292 Model performance of $PM_{2.5}$ in different regions is also different. The model significantly under-
293 predicts $PM_{2.5}$ in the NW and the Other (mostly Southwest cities) regions. Especially in the NW
294 region, MFB value is -0.75 and MFE value is 0.88. $PM_{2.5}$ in all the other regions meets the per-
295 formance criteria. Although most regions meet the model performance criteria in this study, un-
296 der-prediction of $PM_{2.5}$ concentrations are found in all regions (except SCB), as indicated by the
297 large negative MFB values. PM_{10} has similar performance in various regions.



298 Figure 4 illustrates the comparison of predicted and observed monthly averaged $PM_{2.5}$ concentra-
299 tions for all the 60 cities. In NE, the predictions agree well with observations in summer months.
300 Concentrations in fall and winter months are under-predicted, except for Dalian, where the all
301 values are well reproduced. In NCP, the annual trends at most cities are well captured. The mod-
302 el trends to under-predict spring and summer concentrations and over predict December concen-
303 trations. The coastal city, Qingdao, is unique with under-prediction in summer and good estima-
304 tion in other months. In YRD, the model well produces $PM_{2.5}$ for all the months at most sites ex-
305 cept in coastal cities (Zhoushan and Wenzhou) and mountainous cities (Quzhou and Lishui). In
306 SCB, the model underestimates concentrations in the winter months in Chongqing but well esti-
307 mates the concentrations in Chengdu except for March and April. In CEN, the seasonal trend is
308 well captured at all cities but most cities show over-predicted concentrations in December. In NE,
309 $PM_{2.5}$ is uniformly under-predicted. For Other regions, predictions agree with observations at the
310 coastal cities (Fuzhou and Haikou) but concentrations in Lasa are largely under-predicted. The
311 values closest to the observations in the 3×3 surrounding grid cells are similar to the predictions
312 at city centers for most months with clear differences in October, November, and December at
313 several cities. It indicates the higher contributions of primary PM, which has steeper concentra-
314 tion gradients than secondary PM, in winter months than in summer months.

315 Generally, the WRF/CMAQ modeling system with MEIC inventory well reproduces the O_3 and
316 $PM_{2.5}$ concentrations in most regions for most months. Over-prediction of O_3 occurs at low con-
317 centrations in winter while under-prediction of $PM_{2.5}$ happens at low concentration range in
318 summer and in cities in the NW region. The model performance on CO, NO_2 , and SO_2 are also
319 calculated and listed in Tables 3 and 4. There are no performance criteria for these pollutants, but
320 the model performance are in the same ranges as compared to other studies in other coun-
321 tries/regions (Tao et al., 2014a). The model performance at different regions differs due to the
322 differences in emission, topography, and meteorological conditions. The performance on these
323 species can be used as indicator for emission uncertainties. The possible uncertainties are dis-
324 cussed in the *Discussion* section.

325 3.3 Seasonal variations and regional distribution of O_3 and $PM_{2.5}$

326 Figure 5 shows the predicted regional distribution of seasonal averaged O_3 -1h and O_3 -8h. In
327 spring, highest O_3 -1h concentration (~ 100 ppb) occurs in South Asia due to higher temperature,
328 solar radiation and significant amount of emissions from open biomass burning activities (Kondo
329 et al., 2004). Southern China has higher concentrations (~ 70 ppb) than Northern China (~ 50 ppb).
330 However, in summer, NCP has the highest concentration of 80ppb while Southern China (and
331 other regions) has lower concentrations of 50-60 ppb. In fall, most of the regions in China have
332 O_3 -1h concentrations of 50-60 ppb. In winter, NE China and NCP have O_3 -1h concentrations
333 lower than 30ppb while Southern China has the concentrations of 40-50 ppb. In addition to NCP
334 in the summer, SCB is also another hot spot for ozone with high summer and wintertime O_3 -1h
335 of ~ 100 ppb and 60-70 ppb, respectively. O_3 -8h has similar spatial distribution patterns as O_3 -1h
336 for all seasons with lower concentrations (by 5-10 ppb).

337 Figure 6 shows the spatial distribution of seasonal averaged $PM_{2.5}$ concentrations together with
338 the averaged wind vectors as the regional distribution of $PM_{2.5}$ is significantly influenced by
339 wind patterns. In spring, the $PM_{2.5}$ concentrations in China reach approximately $50-70 \mu g m^{-3}$ in
340 Northern, Eastern, and Southern China except coastal provinces of Zhejiang, Fujian, and Guang-



341 dong. It is evident that the high concentrations are related to low wind speed. In summer, the are-
342 as with high $\text{PM}_{2.5}$ concentrations of $\sim 50 \mu\text{g m}^{-3}$ are limited to NCP and SCB while all other re-
343 gions have concentrations of $< 30 \mu\text{g m}^{-3}$. Emissions brought to the NCP by the southerly wind,
344 blockage of dispersion due to mountain ranges to the north and west, and secondary organic aer-
345 osol formed due to strong solar radiation are contributing factors for higher summer $\text{PM}_{2.5}$ in
346 NCP. In fall, the high concentration regions are similar to those in spring but with higher concen-
347 trations of up to $100 \mu\text{g m}^{-3}$ in NCP, YRD, CEN and SCB. In winter, high $\text{PM}_{2.5}$ concentrations
348 are located in the NE, NCP, YRD, CEN and SCB regions. Seasonal average concentrations of
349 more than $200 \mu\text{g m}^{-3}$ occur in large portions of NCP, CEN, and SCB due to low wind speed and
350 mixing height. Strong gradient exists between the high concentration regions and surrounding
351 areas where wind is more lenient to pollutant dispersion.

352 Figure 7 shows the spatial distribution of seasonal averaged $\text{PM}_{2.5}$ components. All components
353 show clear seasonal variations. For secondary inorganic components and anthropogenic primary
354 components (EC and POA), concentrations are usually highest in winter and lowest in summer.
355 Spring and fall concentrations are similar with slightly higher concentrations in fall. For EC and
356 POA, this seasonal variation is largely driven by large increase in the emissions from residential
357 sources in winter, as well as reduced ventilation that is often associated with winter stagnant
358 conditions. For secondary inorganic components, gas phase formation rate of HNO_3 and H_2SO_4
359 decreases as temperature and solar radiation intensity decreases in fall and winter, leading to de-
360 crease in their formation from the homogeneous pathways. However, the amount of secondary
361 NO_3^- and SO_4^{2-} from surface heterogeneous reactions of SO_2 and NO_2 increases as their emis-
362 sions increases, and more particle surface area becomes available due to increase in primary PM
363 concentrations. In addition, ammonium nitrate is preferentially partitioned into the particle phase
364 under colder temperatures (Aw and Kleeman, 2003). In most regions with high concentrations,
365 wintertime NO_3^- concentrations are 150-200% higher than annual average concentrations, while
366 SO_4^{2-} and NH_4^+ concentrations are approximately 100-150% higher (see Figure 8). POA concen-
367 trations in winter are also approximately 100-150% higher in winter than the annual average, es-
368 pecially in northern part of China where residential heating is a significant source of $\text{PM}_{2.5}$ emis-
369 sions. In provinces in southern China with warm temperature, winter POA is not significantly
370 deviated from the annual mean (see Figure 8). Maximum concentrations of NO_3^- and SO_4^{2-} in-
371 crease to beyond $50 \mu\text{g m}^{-3}$ and NH_4^+ as high as $40 \mu\text{g m}^{-3}$ in portions of NCP, CEN, YRD and
372 SCB. This suggests that in large areas, secondary inorganic PM is the most significant contribu-
373 tor to elevated wintertime $\text{PM}_{2.5}$ concentrations. EC has limited spatial distribution since it is on-
374 ly directly emitted. Highest EC concentrations are in NCP, CEN and SCB. The EC concentra-
375 tions are $10\text{-}15 \mu\text{g m}^{-3}$ in winter but lower than $5 \mu\text{g m}^{-3}$ in other seasons. POA concentrations
376 are highly season dependent with the highest concentrations of $\sim 30 \mu\text{g m}^{-3}$ in NCP, CEN, SCB
377 and NE occurring in winter.

378 SOA shows different seasonal variations from the secondary inorganic aerosol and anthropogen-
379 ic primary PM components. In CEN and Eastern China, higher seasonal average SOA concentra-
380 tions of $10\text{-}15 \mu\text{g m}^{-3}$ occur in summer and winter, while in southern China similar levels of SOA
381 occur in spring. The spring and summer high SOA concentrations are dominantly formed from
382 biogenic isoprene emissions but winter SOA is mainly formed from semi-volatile oxidation
383 products of anthropogenic aromatic compounds. Details of SOA formation and composition will
384 be discussed in a separate paper. "Other" components are primary $\text{PM}_{2.5}$ including most part of
385 dust. The concentrations are high in spring, fall and winter. In summary, secondary components



386 have more boarder distribution than primary components. SO_4^{2-} , NO_3^- , NH_4^+ and POA are the
387 most important aerosol components based on their absolute concentrations.

388 **3.4 Temporal variation of $\text{PM}_{2.5}$ components in representative cities**

389 Temporal variations of $\text{PM}_{2.5}$ components are also shown at typical cities in different regions as
390 in Figure 9. The total $\text{PM}_{2.5}$ concentrations in Beijing are high in winter and low in summer with
391 the peak of $\sim 150 \mu\text{g m}^{-3}$ in January. EC contributions are $\sim 5\text{-}10\%$ in winter but less than 5% in
392 other seasons. POA has similar pattern as EC but contributions can be $\sim 35\%$ in winter and $\sim 20\%$
393 in summer. SOA contributions are high in summer with the peak of $\sim 30\%$ in August and very
394 low in winter. SO_4^{2-} and NO_3^- are the top two largest contributors with comparable contributions
395 all the time. NH_4^+ can be as high as $\sim 20\%$ in January and only $\sim 10\%$ in summer. Other compo-
396 nents (“Other”, mostly oxides of crustal elements and other trace metals) contribute up to 15% in
397 some months. In Shanghai, the monthly averaged concentrations are highest in winter and de-
398 crease gradually from spring to fall. Five out of the 12 months are over the Chinese Ambient Air
399 Quality Standards (CAAQS) Grade II standard for 24-hour average $\text{PM}_{2.5}$ ($75 \mu\text{g m}^{-3}$, simply
400 Grade II standard hereafter). EC and POA have similar pattern with a total contribution of 20%
401 in most months. SO_4^{2-} , NO_3^- , and NH_4^+ contribute to more than 70% from November to June and
402 less than 50% in other months, while the contribution of SOA increases significantly to as much
403 as 40% in the summer months. The relative contributions of the “Other” components are about 2
404 times of those in Beijing (15% to 30%). In Guangzhou, the $\text{PM}_{2.5}$ concentrations are lower than
405 Beijing and Shanghai. Predicted $\text{PM}_{2.5}$ concentrations are all within the Grade II standard in Chi-
406 na. Although the contribution of SOA is higher, SO_4^{2-} , NO_3^- , and NH_4^+ are still the major com-
407 ponents with more than 60% contribution all over the year.

408 In Xi’an, the largest city in NW, the differences in $\text{PM}_{2.5}$ at winter and other months are signifi-
409 cant. In winter, the total $\text{PM}_{2.5}$ concentrations are $150\text{-}180 \mu\text{g m}^{-3}$ with POA, SO_4^{2-} , NO_3^- , and
410 NH_4^+ as major components. In Shenyang, a NE city, the $\text{PM}_{2.5}$ concentrations are $\sim 250 \mu\text{g m}^{-3}$ in
411 January followed by $\sim 200 \mu\text{g m}^{-3}$ in February and $\sim 150 \mu\text{g m}^{-3}$ in December. The extremely high
412 concentrations are related to winter residential heating or uncontrolled open biomass (such as
413 straw) burning as can be indicated by the elevated emissions from residential sources. For other
414 seasons, contributions of other components are much lower but contribution of SOA increases to
415 more than 20% ($\sim 10 \mu\text{g m}^{-3}$) in June, likely due to increased biogenic emissions in the densely
416 forested regions in the NE. In Chongqing, located in Sichuan basin, monthly average reaches as
417 high as $230 \mu\text{g m}^{-3}$ in January due to increased atmospheric stability. Spring, summer and fall
418 months have much lower $\text{PM}_{2.5}$ concentrations especially for July, when the $\text{PM}_{2.5}$ is lower than
419 $50 \mu\text{g m}^{-3}$.

420 One of the questions that remain unclear is whether secondary PM formation is enhanced during
421 the high pollution days or high pollution events are simply caused by enhanced emissions and
422 reduced dilution due to stagnant conditions. As an attempt to address this question, Figure 10
423 shows the comparison of relative contributions of $\text{PM}_{2.5}$ components in episode days (\geq the
424 Grade II standard of $75 \mu\text{g m}^{-3}$) and non-episode days. In Guangzhou, there are no episode days
425 predicted, thus only Beijing, Shanghai, Xi’an, Shenyang and Chongqing are included in Figure
426 10. In all cities, the minimum episode-day averaged concentration occurs in summer while the
427 maximum concentration occurs in winter. In most cities and in most seasons, episode days have
428 larger contributions of secondary components (SOA, SO_4^{2-} , NO_3^- , and NH_4^+ , 69.8% on episode



429 days vs. 59.9% on non-episode days) and lower contributions of primary components (EC, POA
430 and Other, 30.2% on episode days vs 40.1% on non-episode days). Some cities show much dras-
431 tic differences in secondary PM contributions between episode and non-episode days. For exam-
432 ple, contribution of secondary PM in Xi'an increases from 40% on non-episode days to more
433 than 60% on episode days in winter. Other cities, such as Chongqing, show less difference in the
434 relative contributions of secondary PM between episode and non-episode days. While most of
435 the secondary PM increase is due to enhanced formation of secondary inorganic components, the
436 contribution of SOA to total PM is significantly higher than that on non-episode days in summer
437 Beijing. This suggests that enhanced SOA formation could also play a significant role in summer
438 PM pollution events of urban areas. In conclusion, in most cities in most seasons, episode days
439 have more rapid formation of secondary PM components than accumulation of primary pollu-
440 tants due to unfavorable weather conditions. This also suggests that controlling the emissions of
441 secondary PM precursors needs to be considered in designing emission control strategies as in
442 many conditions it can be more effective in reducing PM concentrations.

443 4. Discussion

444 Model predicted concentrations of O₃ and PM_{2.5} are evaluated by comparing to ground-level ob-
445 servations at 422 stations in 60 cities in China for ten months in 2013. Predicted concentrations
446 generally agree well with observations, with the model performance statistics meeting the criteria
447 in most of the regions and months. Relatively large bias in model predicted concentrations is
448 found in certain regions in certain months/episodes. Model bias is mainly attributed to uncertain-
449 ties associated with meteorological fields, emissions, model treatment and configurations. Fur-
450 ther studies are still needed to continue improving the model capability in accurately predicting
451 air quality in China.

452 The WRF model performance in this study is comparable to other studies (Hu et al., 2015a;
453 Wang et al., 2010; Wang et al., 2014b; Ying et al., 2014b; Zhang et al., 2012), but a better WRF
454 performance was reported in Zhao et al. (2013b). Mesoscale meteorological modeling studies are
455 also needed to improve the WRF model capability in China. In this study, some meteorological
456 parameters are biased, for example ground-level wind speed is consistently over-predicted and
457 RH is more biased low in winter months (Table 1). A previous study has revealed that air pollu-
458 tion levels are associated with these parameters in highly polluted regions in China (Wang et al.,
459 2014c). It is also demonstrated that bias in predicted meteorological parameters by WRF con-
460 tributes to bias in PM_{2.5} prediction (Hu et al., 2015c). A companion study is undergoing to evalu-
461 ate the sensitivity of air quality predictions to meteorological fields.

462 Uncertainties associated with emission inventory often are the major factor leading to bias in
463 model predictions. The overall good model performance in most regions indicates general accu-
464 racy of the MEIC inventory. However, larger negative bias in CO, NO₂, and SO₂ in NW (Table 4)
465 suggests that anthropogenic emissions, including primary PM_{2.5} are severely under-estimated in
466 this region. Similarly, under-predictions of PM_{2.5} in Lasa are also likely due to under-predictions
467 of anthropogenic emissions, mostly likely those from residential sources. Studies have suggested
468 that dust contributes significantly to PM_{2.5} in NW (Li et al., 2014a; Shen et al., 2009). The cur-
469 rent estimation of dust from wind erosion of natural soil surfaces in the NW is approximately 20
470 μg m⁻³ in spring and lower than 10 μg m⁻³ in other seasons. This relatively low estimation of
471 PM_{2.5} in the NW of China generally agrees with the most recent global long term PM_{2.5} estima-



472 tion based on satellite AOD measurements (Battelle Memorial Institute and Center for
473 International Earth Science Information Network - CIESIN - Columbia University, 2013; de
474 Sherbinin et al., 2014). Emissions of dust from other sources in the urban/rural areas, such as
475 paved and unpaved road and construction activities could be a more important factor that leads to
476 under-predictions of mineral PM components in the NW cities. Both activity data and emission
477 factors used to generate these area emissions should be examined carefully. Source apportion-
478 ment studies based on receptor-oriented techniques should be used to differentiate the contribu-
479 tions from these different dust sources to further constrain the uncertainties in dust emissions.

480 Another important source of under-prediction of PM_{2.5} is SOA, especially in the summer when
481 the biases in PM_{2.5} predictions are larger and more SOA is expected to form due to higher VOCs
482 emissions and higher atmospheric reactivity. While significant progresses have been made to
483 improve model predictions and the SOA module used in the current study has incorporated many
484 of the newly found SOA formation pathways, the understanding of both gas phase and particle
485 phase chemistry that lead to SOA formation is still very limited, and many experimental findings
486 have yet been incorporated by the modeling community. To constrain the uncertainties in SOA
487 predictions, speciated measurements of SOA tracers and gas phase VOC precursors are needed
488 along with models with detailed chemical mechanisms to represent the species. While some
489 VOC speciation data are available, more data in different regions and episodes are needed to im-
490 prove both estimation of VOC emissions and model predictions of SOA.

491 Model grid resolution also contributes to the bias in predictions. The emissions are instantly
492 mixed into 36×36 km² grids after being released from sources. Some of the monitoring stations
493 are located in urban areas near emission sources, such as traffic and industrial facilities, which
494 could imply negative prediction biases when compared with modeled concentrations which rep-
495 resent average concentrations in a grid cell. Higher resolution modeling studies are believed to
496 more accurately capture the concentrations and to reveal finer scale spatial distribution of pollu-
497 tants (Fountoukis et al., 2013; Gan et al., 2016; Stroud et al., 2011). The grid dilution effect theo-
498 retically has larger impact on CO and SO₂ than on O₃ and PM_{2.5}, because O₃ and secondary
499 PM_{2.5} components are often formed regionally and consequently have a more uniform spatial
500 distribution.

501 **5. Conclusion**

502 In this study, O₃ and PM_{2.5} in China during the entire year of 2013 is simulated using an updated
503 WRF/CMAQ model system and anthropogenic emissions from MEIC. The WRF model predicts
504 reasonable meteorological inputs for the CMAQ model. The comparison of predicted and ob-
505 served hourly O₃, peak hour O₃, and daily and monthly averaged PM_{2.5} at 60 cities shows that the
506 current model can successfully reproduces the O₃ and PM_{2.5} concentrations at most cities for
507 most months of the year. Over-prediction of O₃ occurs at low concentration range in winter while
508 under-prediction of PM_{2.5} happens at low concentration range in summer. Spatially, the model
509 has better performance in NE, NCP, Central YRD and SCB but significant under-prediction bi-
510 ases exist for the cities in the NW region. Strong seasonal variations of PM_{2.5} exist and wind
511 speed and direction play important roles in high PM_{2.5} events. Secondary components have more
512 boarder distribution than primary components. Contributions of secondary PM components in-
513 crease during high PM events in a number of urban areas, suggesting that secondary PM for-
514 mation rates are enhanced more than the accumulation rate of primary pollutants. Overall, SO₄²⁻,



515 NO_3^- , NH_4^+ and POA are the most important $\text{PM}_{2.5}$ components. All components have the high-
516 est concentrations in winter except SOA. NCP, CEN and SCB have more severe $\text{PM}_{2.5}$ levels
517 than YRD and PRD.

518 This study reports the detailed model performance of O_3 and $\text{PM}_{2.5}$ in China for an entire year
519 with the public available observations nationwide in China. Although much needs to be done to
520 improve the model performance, this study shows the capability of the model with MEIC emis-
521 sion in reproducing severe air pollution. The concentrations of O_3 , $\text{PM}_{2.5}$ total mass and its chem-
522 ical components from this study will be used in future studies to understand formation mecha-
523 nisms of severe air pollution episodes, investigate the effectiveness of emission control strategies,
524 and estimate human exposure to multiple pollutants for assessing health burden of air pollution
525 in China.

526 **Acknowledgement**

527 This project is partly funded by the Natural Science Foundation of Jiangsu Province
528 (2151071501901 and 2151071508501), Jiangsu Distinguished Professor Project
529 (2191071503201), Jiangsu Six Major Talent Peak Project (2191071502101), the Startup Fund
530 for Talent at NUIST (2243141501008) and the Priority Academic Program Development of
531 Jiangsu Higher Education Institutions (PAPD), Jiangsu Key Laboratory of Atmospheric Envi-
532 ronment Monitoring and Pollution Control of Nanjing University of Information Science and
533 Technology, and Jiangsu Province Innovation Platform for Superiority Subject of Environmental
534 Science and Engineering (No. KHK1201). We would like to thank the computation resources
535 from the Texas A&M Supercomputing Facility (<http://sc.tamu.edu/>) for completing some of the
536 model simulations reported in this study.

537 **References**

- 538 Aw, J. and Kleeman, M.J., 2003. Evaluating the first-order effect of intraannual temperature variability
539 on urban air pollution. *Journal of Geophysical Research: Atmospheres*, 108(D12): 4365.
- 540 Battelle Memorial Institute and Center for International Earth Science Information Network - CIESIN -
541 Columbia University, 2013. Global Annual Average PM2.5 Grids from MODIS and MISR Aerosol
542 Optical Depth (AOD). NASA Socioeconomic Data and Applications Center (SEDAC), Palisades, NY.
- 543 Carter, W.P.L., 2010. Development of the SAPRC-07 chemical mechanism. *Atmos. Environ.*, 44(3): 5324-
544 5335.
- 545 Carter, W.P.L. and Heo, G., 2012. Development of revised SAPRC aromatics mechanisms. Final Report to
546 the California Air Resources Board, Contracts No. 07-730 and 08-326, April 12, 2012. .
- 547 de Sherbinin, A., Levy, M., Zell, E., Weber, S. and Jaiteh, M., 2014. Using Satellite Data to Develop
548 Environmental Indicators. *Environmental Research Letters*, 9(8).
- 549 Emery, C. et al., 2012. Regional and global modeling estimates of policy relevant background ozone over
550 the United States. *Atmospheric Environment*, 47(0): 206-217.
- 551 Emery, C., Tai, E. and Yarwood, G., 2001. Enhanced meteorological modeling and performance
552 evaluation for two Texas episodes, Novato, CA.
- 553 EPA, U.S., 2005. Guidance on the Use of Models and Other Analyses in Attainment Demonstrations for
554 the 8-hour Ozone NAAQS. EPA-454/R-05-002.
- 555 Fountoukis, C. et al., 2013. Impact of grid resolution on the predicted fine PM by a regional 3-D chemical
556 transport model. *Atmospheric Environment*, 68: 24-32.
- 557 Fu, T.M. et al., 2008. Global budgets of atmospheric glyoxal and methylglyoxal, and implications for
558 formation of secondary organic aerosols. *J Geophys Res-Atmos*, 113(D15).
- 559 Gan, C.-M. et al., 2016. Assessment of the effects of horizontal grid resolution on long-term air quality
560 trends using coupled WRF-CMAQ simulations. *Atmospheric Environment*, 132: 207-216.
- 561 Hildebrandt, L., Donahue, N.M. and Pandis, S.N., 2009. High formation of secondary organic aerosol
562 from the photo-oxidation of toluene. *Atmos. Chem. Phys.*, 9(9): 2973-2986.
- 563 Hu, J., Wang, Y., Ying, Q. and Zhang, H., 2014a. Spatial and temporal variability of PM2.5 and PM10 over
564 the North China Plain and the Yangtze River Delta, China. *Atmospheric Environment*, 95(0): 598-
565 609.
- 566 Hu, J. et al., 2015a. Source contributions and regional transport of primary particulate matter in China.
567 *Environmental Pollution*, 207: 31-42.
- 568 Hu, J., Ying, Q., Wang, Y. and Zhang, H., 2015b. Characterizing multi-pollutant air pollution in China:
569 Comparison of three air quality indices. *Environ Int*, 84: 17-25.
- 570 Hu, J. et al., 2015c. Long-term particulate matter modeling for health effect studies in California - Part I:
571 model performance on temporal and spatial variations. *Atmos Chem Phys*, 15: 3445-3461.
- 572 Hu, X.-M. et al., 2014b. Impact of the Loess Plateau on the atmospheric boundary layer structure and air
573 quality in the North China Plain: A case study. *Science of The Total Environment*, 499: 228-237.
- 574 Jacob, D.J. and Winner, D.A., 2009. Effect of climate change on air quality. *Atmospheric Environment*,
575 43(1): 51-63.
- 576 Kondo, Y. et al., 2004. Impacts of biomass burning in Southeast Asia on ozone and reactive nitrogen over
577 the western Pacific in spring. *Journal of Geophysical Research: Atmospheres*, 109(D15): n/a-n/a.
- 578 Kurokawa, J. et al., 2013. Emissions of air pollutants and greenhouse gases over Asian regions during
579 2000–2008: Regional Emission inventory in ASia (REAS) version 2. *Atmos. Chem. Phys.*, 13(21):
580 11019-11058.
- 581 Lei, Y., Zhang, Q., Nielsen, C. and He, K., 2011. An inventory of primary air pollutants and CO2 emissions
582 from cement production in China, 1990–2020. *Atmospheric Environment*, 45(1): 147-154.
- 583 Li, J. et al., 2015a. Modeling regional secondary organic aerosol using the Master Chemical Mechanism.
584 *Atmos Environ*, 102: 52-61.



- 585 Li, J. et al., 2014a. Comparison of abundances, compositions and sources of elements, inorganic ions and
586 organic compounds in atmospheric aerosols from Xi'an and New Delhi, two megacities in China
587 and India. *Science of The Total Environment*, 476–477(0): 485-495.
- 588 Li, M. et al., 2014b. Mapping Asian anthropogenic emissions of non-methane volatile organic
589 compounds to multiple chemical mechanisms. *Atmos. Chem. Phys.*, 14(11): 5617-5638.
- 590 Li, X. et al., 2015b. Source contributions of urban PM_{2.5} in the Beijing–Tianjin–Hebei region: Changes
591 between 2006 and 2013 and relative impacts of emissions and meteorology. *Atmos Environ*, In
592 press.
- 593 Lin, Y.-H. et al., 2013. Epoxide as a precursor to secondary organic aerosol formation from isoprene
594 photooxidation in the presence of nitrogen oxides. *Proceedings of the National Academy of
595 Sciences*, 110(17): 6718-6723.
- 596 Menon, S. et al., 2008. Aerosol climate effects and air quality impacts from 1980 to 2030. *Environmental
597 Research Letters*, 3(2): 024004.
- 598 Ng, N.L. et al., 2007. Secondary organic aerosol formation from m-xylene, toluene, and benzene.
599 *Atmospheric Chemistry and Physics*, 7: 3909-3922.
- 600 Poschl, U., 2005. Atmospheric aerosols: Composition, transformation, climate and health effects.
601 *Angewandte Chemie-International Edition*, 44(46): 7520-7540.
- 602 Pui, D.Y.H., Chen, S.-C. and Zuo, Z., 2014. PM_{2.5} in China: Measurements, sources, visibility and health
603 effects, and mitigation. *Particuology*, 13(0): 1-26.
- 604 Qiao, X. et al., 2015. Modeling dry and wet deposition of sulfate, nitrate, and ammonium ions in
605 Jiuzhaigou National Nature Reserve, China using a source-oriented CMAQ model: Part I. Base
606 case model results. *Sci Total Environ*, 532: 831-839.
- 607 Shen, Z. et al., 2009. Ionic composition of TSP and PM_{2.5} during dust storms and air pollution episodes
608 at Xi'an, China. *Atmospheric Environment*, 43(18): 2911-2918.
- 609 Stroud, C.A. et al., 2011. Impact of model grid spacing on regional- and urban- scale air quality
610 predictions of organic aerosol. *Atmos. Chem. Phys.*, 11(7): 3107-3118.
- 611 Sun, Y. et al., 2014. Investigation of the sources and evolution processes of severe haze pollution in
612 Beijing in January 2013. *Journal of Geophysical Research: Atmospheres*, 119(7): 2014JD021641.
- 613 Tao, J. et al., 2014a. PM_{2.5} pollution in a megacity of southwest China: source apportionment and
614 implication. *Atmos. Chem. Phys.*, 14(16): 8679-8699.
- 615 Tao, M. et al., 2014b. Formation process of the widespread extreme haze pollution over northern China
616 in January 2013: Implications for regional air quality and climate. *Atmospheric Environment*,
617 98(0): 417-425.
- 618 Wang, D. et al., 2014a. Source contributions to primary and secondary inorganic particulate matter
619 during a severe wintertime PM_{2.5} pollution episode in Xi'an, China. *Atmospheric Environment*,
620 97(0): 182-194.
- 621 Wang, L.T. et al., 2010. Assessment of air quality benefits from national air pollution control policies in
622 China. Part I: Background, emission scenarios and evaluation of meteorological predictions.
623 *Atmospheric Environment*, 44: 3442-3448.
- 624 Wang, L.T. et al., 2014b. The 2013 severe haze over southern Hebei, China: model evaluation, source
625 apportionment, and policy implications. *Atmospheric Chemistry and Physics*, 14(6): 3151-3173.
- 626 Wang, S.W. et al., 2012. Growth in NO_x emissions from power plants in China: bottom-up estimates and
627 satellite observations. *Atmos. Chem. Phys.*, 12(10): 4429-4447.
- 628 Wang, Y., Ying, Q., Hu, J. and Zhang, H., 2014c. Spatial and temporal variations of six criteria air
629 pollutants in 31 provincial capital cities in China during 2013–2014. *Environment International*,
630 73(0): 413-422.
- 631 Wiedinmyer, C. et al., 2011. The Fire INventory from NCAR (FINN): a high resolution global model to
632 estimate the emissions from open burning. *Geoscientific Model Development*, 4: 625-641.



- 633 Ying, Q. et al., 2014a. Impacts of Stabilized Criegee Intermediates, surface uptake processes and higher
634 aromatic secondary organic aerosol yields on predicted PM_{2.5} concentrations in the Mexico City
635 Metropolitan Zone. *Atmos Environ*, 94(0): 438-447.
- 636 Ying, Q., Li, J. and Kota, S.H., 2015. Significant Contributions of Isoprene to Summertime Secondary
637 Organic Aerosol in Eastern United States. *Environmental Science & Technology*, 49(13): 7834-
638 7842.
- 639 Ying, Q., Wu, L. and Zhang, H., 2014b. Local and inter-regional contributions to PM_{2.5} nitrate and sulfate
640 in China. *Atmospheric Environment*, 94(0): 582-592.
- 641 Zhang, B., Wang, Y. and Hao, J., 2015a. Simulating aerosol–radiation–cloud feedbacks on meteorology
642 and air quality over eastern China under severe haze conditions in winter. *Atmos. Chem. Phys.*,
643 15(5): 2387-2404.
- 644 Zhang, H. et al., 2012. Source apportionment of PM_{2.5} nitrate and sulfate in China using a source-
645 oriented chemical transport model. *Atmos. Environ.*, 62(0): 228-242.
- 646 Zhang, H., Wang, Y., Hu, J., Ying, Q. and Hu, X.-M., 2015b. Relationships between meteorological
647 parameters and criteria air pollutants in three megacities in China. *Environmental Research*,
648 140(0): 242-254.
- 649 Zhang, X. et al., 2014. Influence of vapor wall loss in laboratory chambers on yields of secondary organic
650 aerosol. *Proceedings of the National Academy of Sciences*, 111(16): 5802-5807.
- 651 Zhao, B. et al., 2013a. Environmental effects of the recent emission changes in China: implications for
652 particulate matter pollution and soil acidification. *Environmental Research Letters*, 8(2): 024031.
- 653 Zhao, B. et al., 2013b. Environmental effects of the recent emission changes in China: implications for
654 particulate matter pollution and soil acidification. *Environmental Research Letters*, 8(2).
- 655 Zheng, B. et al., 2014. High-resolution mapping of vehicle emissions in China in 2008. *Atmos. Chem.*
656 *Phys.*, 14(18): 9787-9805.
- 657 Zheng, B. et al., 2015. Heterogeneous chemistry: a mechanism missing in current models to explain
658 secondary inorganic aerosol formation during the January 2013 haze episode in North China.
659 *Atmos. Chem. Phys.*, 15(4): 2031-2049.

660

661



662 Table 1. Meteorology performance in all the months in 2013 (OBS, mean observation; PRE,
 663 mean prediction; MB, mean bias; GE, gross error; and RMSE, root mean square error). The
 664 benchmarks are suggested by Emery et al. (2001) for the MM5 model in the East US with 4-
 665 12km grid resolution. The values that do not meet the criteria are shaded.

		Jan	Feb	Mar	Apr	May	Jun	Jul	Aug	Sep	Oct	Nov	Dec	Bench- mark
T2 (K)	OBS	267.3	270.4	277.5	282.7	289.3	293.9	297.0	297.1	292.1	286.0	278.1	272.8	
	PRE	266.1	268.9	276.2	281.8	288.7	293.6	296.5	296.5	291.9	286.0	278.4	273.1	
	MB	1.2	-1.4	-1.3	-0.8	-0.7	-0.3	-0.5	-0.6	-0.2	0.0	0.3	0.3	≤±0.5
	GE	3.7	3.3	3.0	2.7	2.7	2.7	2.6	2.5	2.4	2.5	2.7	2.8	≤2.0
	RMSE	4.7	4.5	4.0	3.6	3.5	3.6	3.5	3.3	3.2	3.3	3.5	3.8	
WS (ms ⁻¹)	OBS	3.0	3.5	3.7	3.8	3.6	3.3	3.4	3.2	3.3	3.4	3.5	3.5	
	PRE	3.2	4.8	4.8	4.8	4.4	3.8	4.0	3.8	4.0	4.4	4.6	4.7	
	MB	0.2	1.3	1.1	1.0	0.7	0.5	0.6	0.5	0.7	1.0	1.1	1.2	≤±0.5
	GE	1.3	2.0	1.9	1.9	1.7	1.53	1.6	1.5	1.6	1.7	1.9	1.9	≤2.0
	RMSE	2.6	2.6	2.5	2.4	2.2	2.0	2.0	1.9	2.1	2.3	2.4	2.5	≤2.0
WD (°)	OBS	187.5	212.0	205.0	202.4	187.3	171.2	187.0	190.6	174.8	183.0	216.0	216.4	
	PRE	209.9	229.1	220.4	216.8	198.5	175.8	200.8	203.4	171.4	182.1	236.5	234.0	
	MB	10.5	17.1	15.4	14.4	11.2	4.6	13.8	12.9	-3.4	-0.9	20.5	17.7	≤±10
	GE	46.3	47.7	46.7	44.8	46.2	49.4	46.6	47.4	47.5	45.6	44.8	46.6	≤±30
	RMSE	66.3	65.1	64.1	62.1	63.4	66.4	63.5	64.4	65.0	62.9	61.8	63.8	
RH (%)	OBS	64.9	78.9	69.5	67.1	64.3	68.7	70.8	70.4	69.38	71.7	72.2	75.3	
	PRE	63.6	73.4	68.4	65.3	64.0	68.1	72.0	72.1	69.2	71.0	68.9	68.7	
	MB	-1.4	-5.6	-1.1	-1.8	-0.3	-0.5	1.2	1.7	-0.6	-0.7	-3.3	-6.5	
	GE	19.2	14.1	15.4	14.9	14.5	13.4	13.5	13.0	12.6	13.5	14.1	14.8	
	RMSE	21.2	18.3	19.4	18.9	18.6	17.4	17.3	16.6	16.3	17.4	18.4	19.8	

666



667 Table 2. List of the cities in different regions with available observations.

Region	City list
Northeast (4 cities)	1. Harbin, 2. Changchun, 3. Shenyang, 4. Dalian
North China Plain (NCP) (14)	5. Chengde, 6. Beijing, 7. Qinhuangdao, 8. Tangshan, 9. Langfang, 10. Tianjin, 11. Baoding, 12. Cangzhou, 13. Shijiazhuang, 14. Hengshui, 15. Handan, 16. Jinan, 17. Qingdao, 28. Huhehaote
Yangtze River Delta (YRD) (20)	21. Lianyungang, 22. Suqian, 23. Xuzhou, 24. Huai'an, 25. Taizhou, 26. Yangzhou, 27. Nanjing, 29. Nantong, 30. Suzhou, 31. Wuxi, 32. Shanghai, 33. Huzhou, 34. Hangzhou, 35. Jiaxing, 36. Shaoxing, 37. Zhoushan, 38. Wenzhou, 39. Jinhua, 40. Quzhou, 41. Lishui
Pearl River Delta (PRD) (3)	46. Guangzhou, 47. Zhuhai, 60. Shenzhen
Central China (6)	18. Taiyuan, 19. Zhengzhou, 20. Hefei, 43. Wuhan, 44. Nanchang, 45. Changsha
Northwest (5)	54. Xi'an, 55. Yinchuan, 56. Lanzhou, 57. Xining, 58. Wulumuqi
Sichuan basin (SCB) (2)	52. Chongqing, 53. Chengdu
Southwest+Other (6)	42. Fuzhou, 48. Haikou, 49. Nanning, 50. Kunming, 51. Guiyang, 59. Lasa

668



669 Table 3. Model performance on O₃-1h, O₃-8h, PM_{2.5}, PM₁₀, CO, NO₂, and SO₂ in March to De-
 670 cember 2013 (OBS, mean observation; PRE, mean prediction; MFB, mean fractional bias; MFE,
 671 mean fractional error; MNB, mean normalized bias; MNE, mean normalized error). The perfor-
 672 mance criteria for PM_{2.5} are suggested by EPA (2007), and the performance criteria for O₃ are
 673 suggested by EPA (2005). The values that do not meet the criteria are shaded.

		Mar	Apr	May	Jun	Jul	Aug	Sep	Oct	Nov	Dec	Criteria
O ₃ -1h (ppb)	OBS	53.96	57.73	65.37	67.72	65.7	68.3	60.73	57.97	49.18	46.53	
	PRE	58.09	61.76	66.91	67.82	63.23	66.47	59.5	54.92	45.66	42.09	
	MFB	0.08	0.09	0.05	0.01	-0.01	-0.01	0.01	-0.03	-0.05	-0.09	
	MFE	0.29	0.27	0.25	0.3	0.29	0.28	0.27	0.26	0.27	0.32	
	MNB	0.16	0.17	0.11	0.1	0.06	0.06	0.07	0.03	0.01	-0.01	≲ ±0.15
	MNE	0.34	0.32	0.28	0.33	0.31	0.3	0.29	0.26	0.26	0.28	≲ 0.3
O ₃ -8h (ppb)	OBS	50.4	47.44	52.59	54.36	51.79	54.03	48.63	48.03	40.31	38.92	
	PRE	48.81	51.49	57.86	59.58	54.05	58.07	50.64	48.48	40.6	40.7	
	MFB	-0.05	0.07	0.1	0.08	0.03	0.06	0.04	0.01	-0.01	0.01	
	MFE	0.29	0.24	0.24	0.28	0.26	0.26	0.25	0.24	0.25	0.27	
	MNB	0.03	0.13	0.16	0.16	0.09	0.12	0.1	0.06	0.03	0.07	≲ ±0.15
	MNE	0.29	0.28	0.28	0.32	0.28	0.29	0.27	0.25	0.24	0.27	≲ 0.3
PM _{2.5} (μg m ⁻³)	OBS	81.68	62.07	60.12	60.83	45.52	47.1	56.08	85.69	88.93	123.73	
	PRE	66.12	43.24	39.28	41.6	31.31	39.07	52.24	56.09	80.21	126.83	
	MFB	-0.24	-0.4	-0.47	-0.41	-0.48	-0.31	-0.21	-0.42	-0.17	-0.07	≲ ±0.6
	MFE	0.59	0.63	0.68	0.69	0.72	0.65	0.62	0.64	0.6	0.59	≲ 0.75
	MNB	0.04	-0.16	-0.19	-0.09	-0.17	-0.01	0.11	-0.16	0.17	0.3	
	MNE	0.61	0.54	0.58	0.63	0.63	0.64	0.68	0.56	0.7	0.75	
PM ₁₀ (μg m ⁻³)	OBS	151.39	121.56	111.90	96.95	79.90	85.04	98.27	136.02	150.27	178.78	
	PRE	74.72	52.48	45.37	46.58	35.59	44.63	57.53	65.12	90.22	136.26	
	MFB	-0.59	-0.73	-0.79	-0.68	-0.78	-0.65	-0.54	-0.65	-0.48	-0.34	
	MFE	0.74	0.83	0.89	0.82	0.88	0.79	0.73	0.77	0.72	0.63	
	MNB	-0.31	-0.43	-0.45	-0.35	-0.44	-0.35	-0.24	-0.36	-0.16	-0.04	
	MNE	0.56	0.58	0.62	0.62	0.63	0.59	0.60	0.59	0.64	0.62	
CO (ppm)	OBS	1.17	0.94	0.86	0.8	0.73	0.75	0.85	1.09	1.16	1.48	
	PRE	0.37	0.26	0.25	0.26	0.23	0.25	0.29	0.31	0.41	0.59	
	MFB	-0.89	-0.97	-0.97	-0.91	-0.95	-0.92	-0.9	-0.98	-0.88	-0.8	
	MFE	0.95	1.01	1	0.95	0.99	0.96	0.95	1.02	0.92	0.86	
	MNB	-0.54	-0.6	-0.6	-0.56	-0.58	-0.56	-0.56	-0.61	-0.54	-0.49	
	MNE	0.63	0.65	0.65	0.63	0.64	0.63	0.63	0.66	0.62	0.59	
NO ₂ (ppb)	OBS	23.33	21.26	19.83	18.11	16.34	16.5	19.74	24.82	27.41	31.41	
	PRE	10.11	8.87	8.51	8.74	8.12	8.77	10.45	11.85	13.45	13.87	
	MFB	-0.83	-0.88	-0.86	-0.79	-0.79	-0.73	-0.71	-0.76	-0.7	-0.77	
	MFE	0.94	0.99	0.99	0.95	0.95	0.91	0.89	0.91	0.85	0.87	
	MNB	-0.45	-0.48	-0.46	-0.4	-0.4	-0.35	-0.35	-0.39	-0.37	-0.44	
	MNE	0.65	0.67	0.68	0.68	0.68	0.67	0.66	0.65	0.62	0.61	
SO ₂ (ppb)	OBS	19.1	15.8	15.25	12.93	12.32	12.96	13.24	15.53	21.74	27.88	
	PRE	11.64	8.87	8.31	8.61	7.09	8.88	11.94	14.25	17.91	23.32	
	MFB	-0.61	-0.66	-0.68	-0.59	-0.73	-0.56	-0.39	-0.29	-0.31	-0.32	
	MFE	0.89	0.9	0.91	0.89	0.98	0.89	0.84	0.78	0.82	0.83	
	MNB	-0.14	-0.23	-0.23	-0.11	-0.22	-0.08	0.23	0.25	0.29	0.31	
	MNE	0.79	0.74	0.76	0.8	0.81	0.82	1	0.95	1.01	1.03	

674

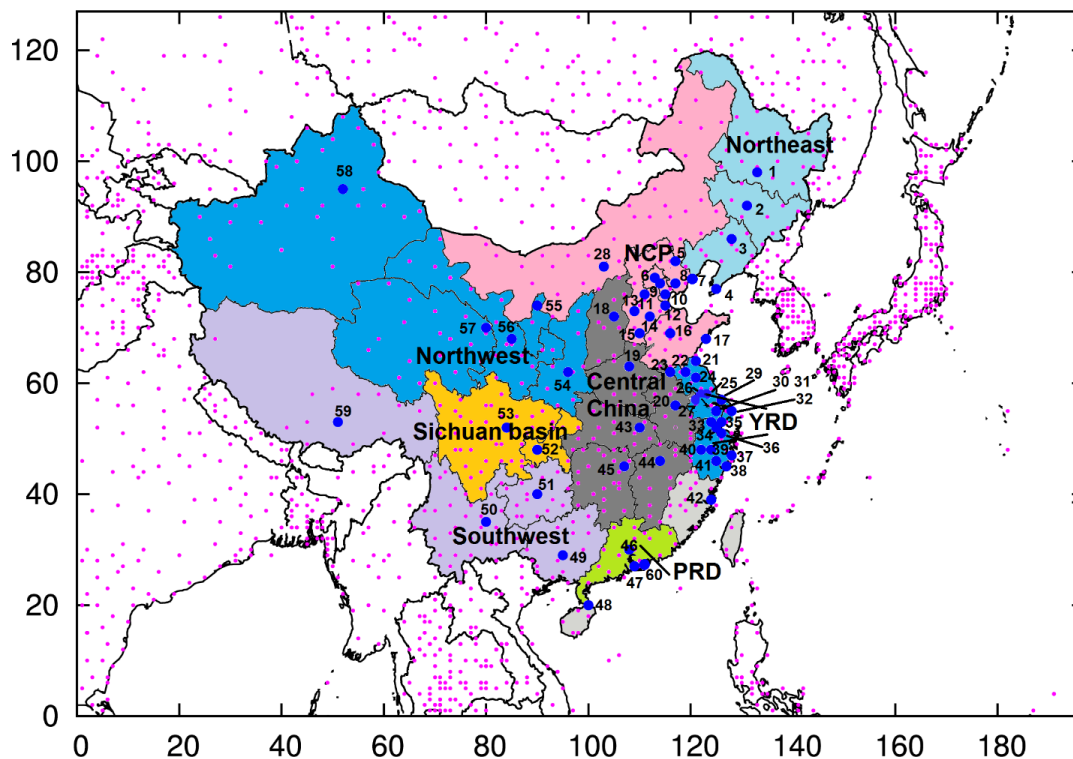


675 Table 4. Model performance on O₃-1h, O₃-8h, PM_{2.5}, PM₁₀, CO, NO₂, and SO₂ in different re-
 676 gions during March to December, 2013. The values that do not meet the criteria are shaded.

		NCP	YRD	PRD	SCB	NE	CEN	NW	Other
O ₃ -1h (ppb)	OBS	65.18	63.84	65.7	67.85	53.37	63.1	54.5	54.21
	PRE	65.84	59.02	56.6	71.36	57.9	62.79	60.5	55.37
	MFB	0.03	-0.07	-0.13	0.08	0.09	0.03	0.14	0.05
	MFE	0.27	0.27	0.3	0.31	0.24	0.31	0.28	0.28
	MNB	0.1	-0.01	-0.06	0.18	0.14	0.12	0.22	0.13
	MNE	0.3	0.26	0.29	0.36	0.27	0.34	0.33	0.3
O ₃ -8h (ppb)	OBS	53.38	52.96	51.25	53.48	46.73	49.88	44.26	45
	PRE	57.51	51.72	46.13	59.04	52.18	54.33	52.67	49.94
	MFB	0.06	-0.03	-0.11	0.1	0.1	0.08	0.18	0.1
	MFE	0.26	0.26	0.26	0.26	0.23	0.26	0.28	0.24
	MNB	0.13	0.02	-0.06	0.17	0.15	0.15	0.25	0.16
	MNE	0.3	0.26	0.24	0.3	0.26	0.3	0.33	0.28
PM _{2.5} (μg m ⁻³)	OBS	90.85	65.55	49.28	65.61	60.93	77.74	70.13	42.7
	PRE	65.5	55.55	29.19	78.83	48.57	74.95	33.84	33.55
	MFB	-0.33	-0.27	-0.56	0.05	-0.26	-0.16	-0.75	-0.53
	MFE	0.64	0.57	0.68	0.57	0.62	0.57	0.88	0.77
	MNB	-0.01	-0.04	-0.33	0.47	0.03	0.15	-0.39	-0.2
	MNE	0.65	0.54	0.52	0.84	0.63	0.66	0.65	0.63
PM ₁₀ (μg m ⁻³)	OBS	164.80	104.94	69.85	104.79	99.08	122.64	143.95	68.67
	PRE	73.69	63.47	34.20	86.70	52.80	80.44	44.25	35.63
	MFB	-0.71	-0.55	-0.69	-0.25	-0.62	-0.49	-0.98	-0.76
	MFE	0.84	0.70	0.77	0.62	0.78	0.70	1.05	0.87
	MNB	-0.37	-0.30	-0.43	0.07	-0.32	-0.20	-0.56	-0.42
	MNE	0.63	0.54	0.55	0.68	0.60	0.60	0.69	0.62
CO (ppm)	OBS	1.22	0.8	0.81	0.82	0.79	1.11	1.13	0.75
	PRE	0.37	0.29	0.22	0.41	0.25	0.4	0.23	0.22
	MFB	-0.89	-0.86	-1.11	-0.62	-0.93	-0.87	-1.21	-1.04
	MFE	0.95	0.9	1.12	0.71	0.96	0.93	1.22	1.07
	MNB	-0.54	-0.55	-0.69	-0.39	-0.58	-0.52	-0.72	-0.63
	MNE	0.63	0.6	0.7	0.52	0.63	0.62	0.74	0.68
NO ₂ (ppb)	OBS	24.28	21.42	23.12	21.2	21.09	21.01	22.23	16.2
	PRE	11.26	11.77	10.71	12.53	6.37	12.03	8.4	4.29
	MFB	-0.72	-0.65	-0.7	-0.56	-1.09	-0.62	-0.95	-1.24
	MFE	0.85	0.83	0.83	0.78	1.15	0.83	1.05	1.28
	MNB	-0.39	-0.31	-0.39	-0.24	-0.61	-0.27	-0.52	-0.7
	MNE	0.62	0.63	0.6	0.62	0.73	0.66	0.69	0.75
SO ₂ (ppb)	OBS	22.31	14.07	10.41	12.83	21.06	17.26	16.66	11.81
	PRE	12.24	8.66	8.07	25.77	5.13	18.55	11.58	10.28
	MFB	-0.57	-0.62	-0.45	0.34	-1.14	-0.24	-0.6	-0.63
	MFE	0.8	0.87	0.77	0.73	1.21	0.8	0.95	1
	MNB	-0.21	-0.22	-0.1	1.5	-0.61	0.46	-0.07	-0.02
	MNE	0.66	0.71	0.69	1.78	0.76	1.13	0.86	0.94



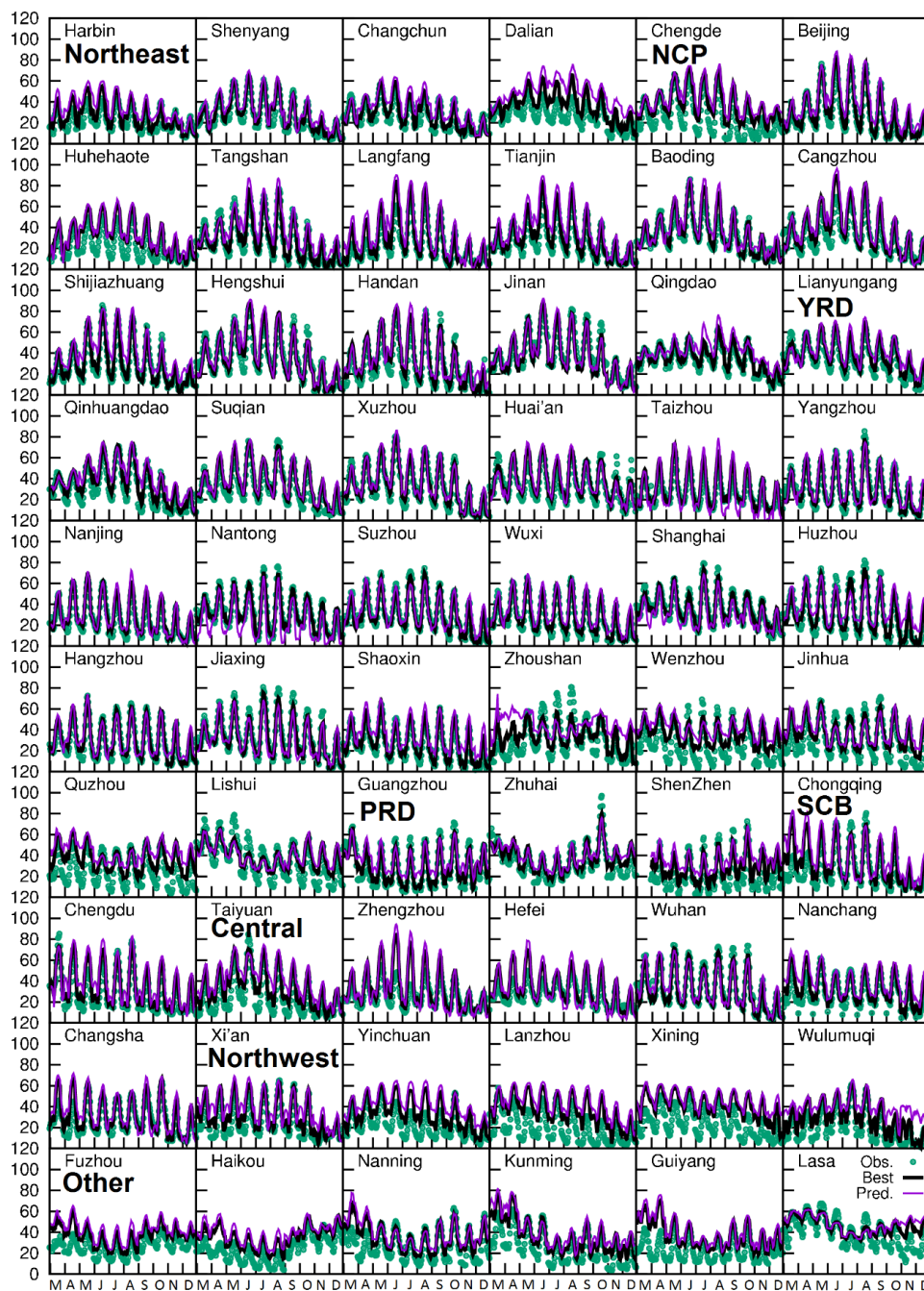
677



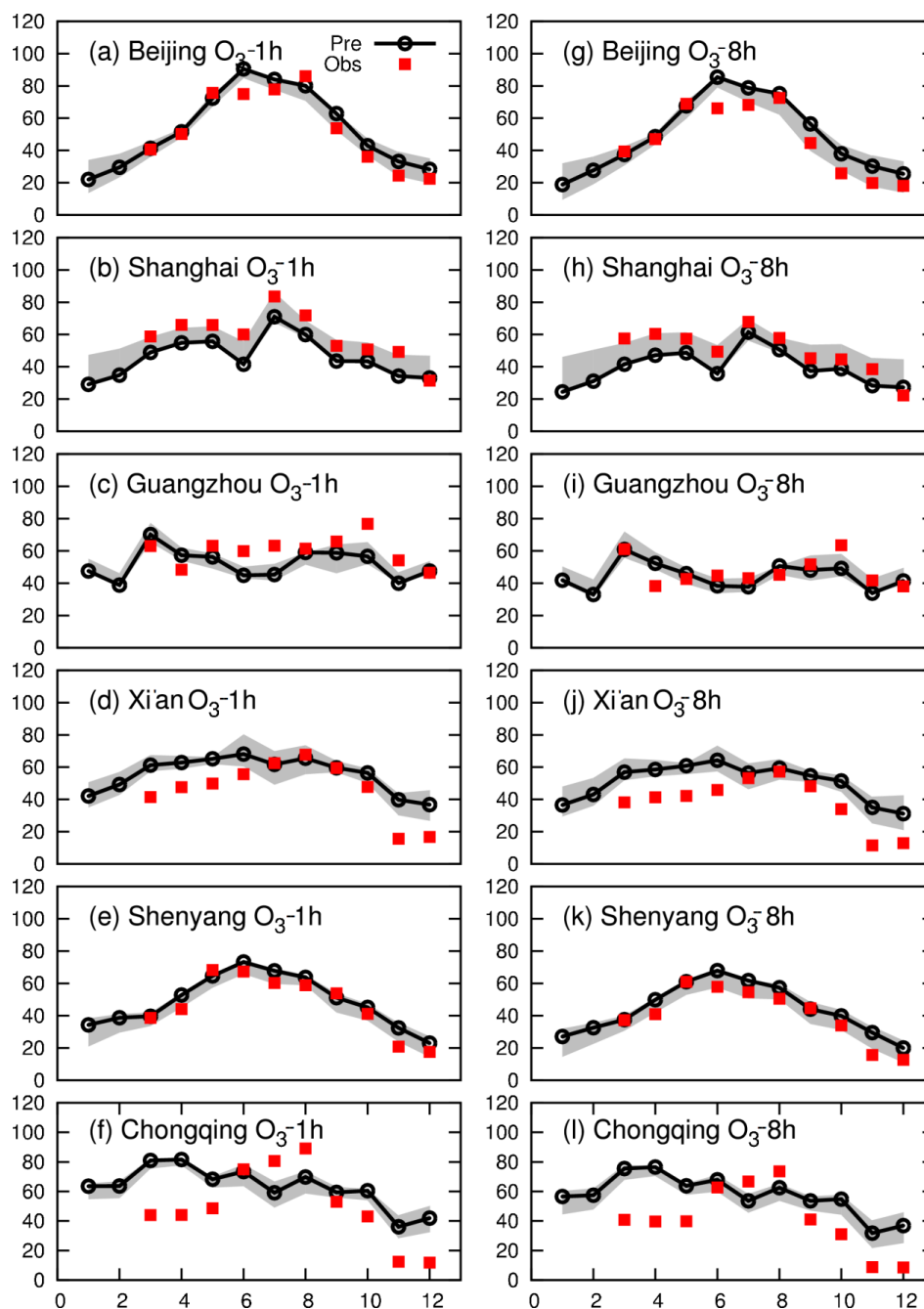
678

679

680 Figure 1. Model domain. The axes are the number of grid cells. Blue filled circles show the loca-
681 tions of cities with air quality observations (see Table 2). The purple dots show the locations of
682 meteorological stations. The figure also shows the regions discussed in the text for better under-
683 standing. NCP represents North China Plain, YRD represents Yangtze River Delta, and PRD
684 represents Pearl River Delta.
685

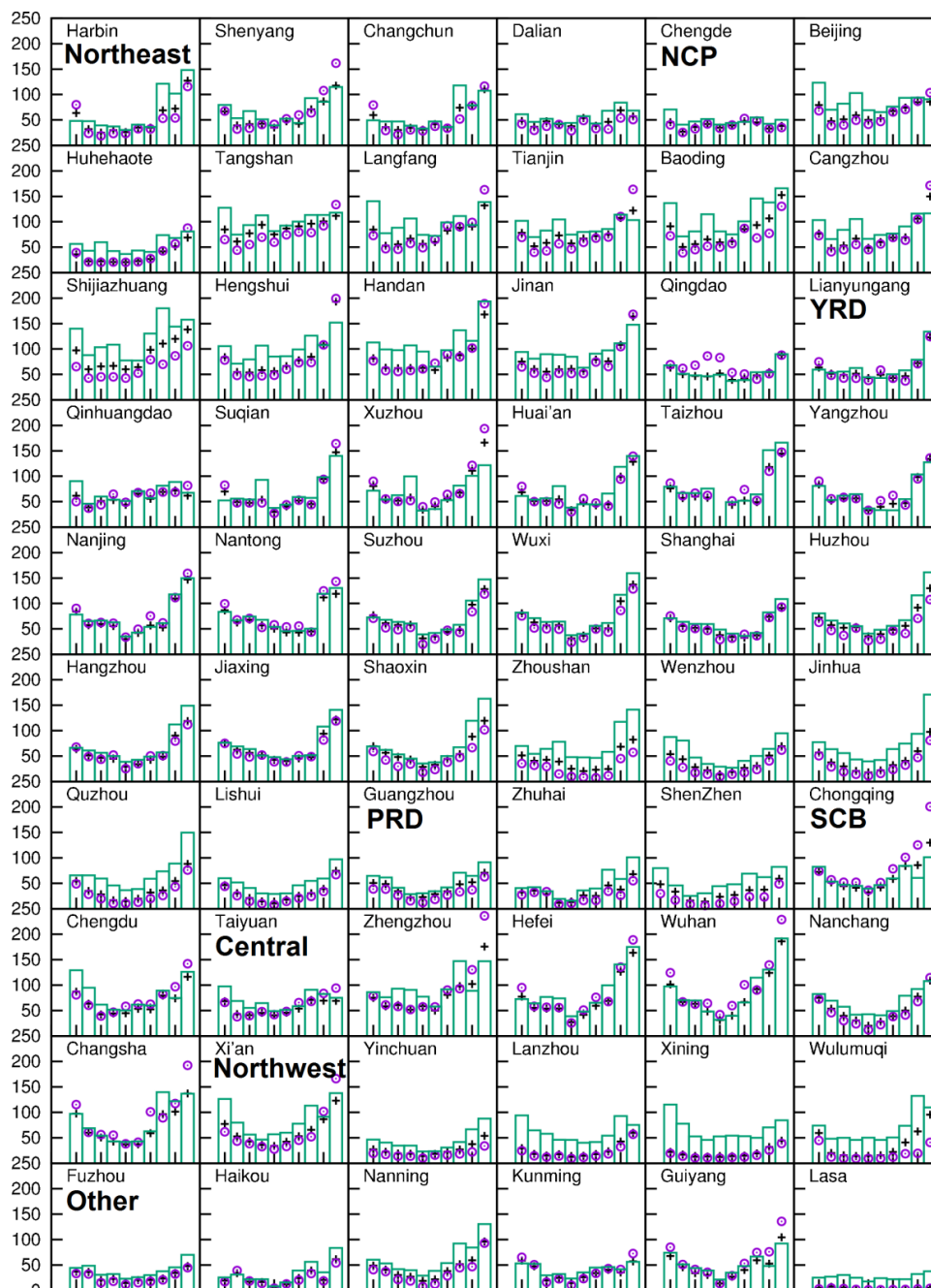


686
 687 Figure 2. Comparison of monthly averaged diurnal variations of O₃ concentrations from March to De-
 688 cember, 2013. Pred. are the values predicted at the grid cell each city center located while Best are the
 689 values predicted closest to the observations within 3 by 3 grid cell regions that surround the observation.
 690 Units are ppb.



691

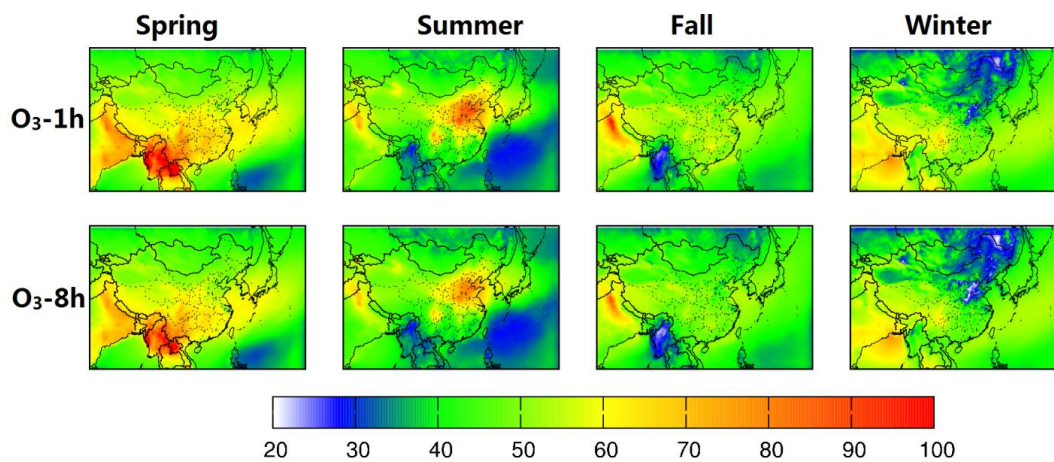
692 Figure 2. Comparison of predicted and observed O₃-1h and O₃-8h concentrations at Beijing, Shanghai,
693 Guangzhou, Xi'an, Shenyang, and Chongqing. Grey areas represent ranges in model predictions within
694 3x3 grid cells surrounding the observation Units are ppb.



695
 696 Figure 4. Comparison of predicted (in column) and observed (in circle) monthly averaged $PM_{2.5}$ concentra-
 697 tions for March to December, 2013. The “Best” lines (in “+”) represent predictions closest to the hour-
 698 ly observations within a 3×3 grid cell region with the grid cell where the monitoring sites are located at
 699 the center. Units are $\mu g m^{-3}$.

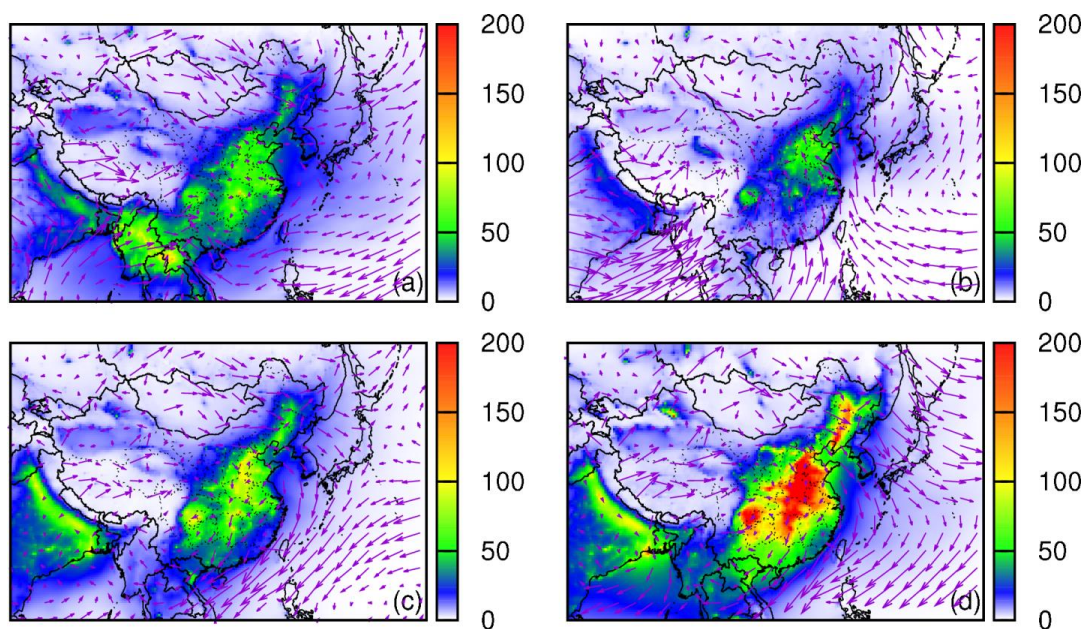


700



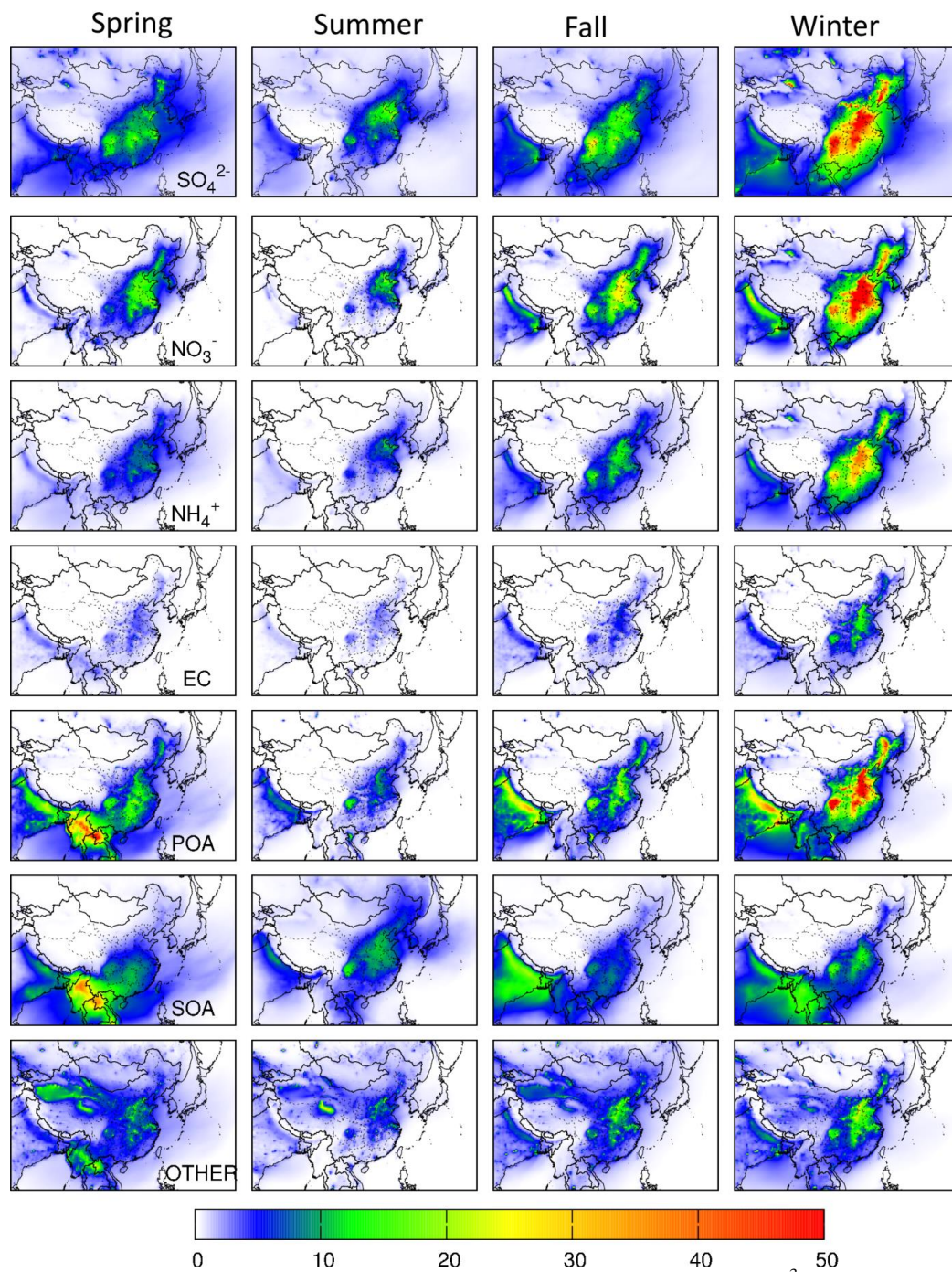
701
702

Figure 5. Seasonal variations of predicted regional distribution of O₃-1h and O₃-8h. Units are ppb.



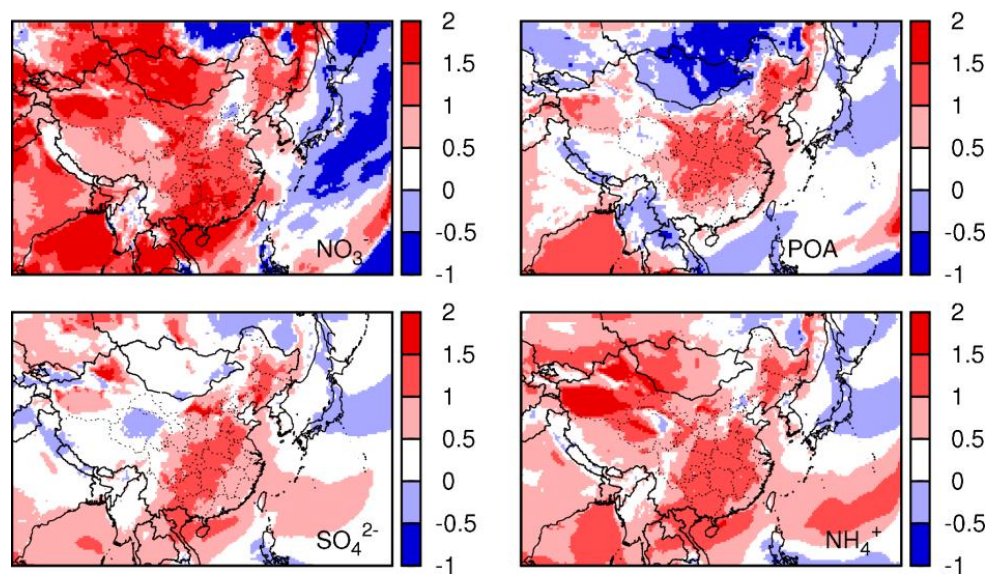
703
704
705

Figure 6. Seasonal variation of predicted $\text{PM}_{2.5}$ and wind vectors: (a) spring, (b) summer, (c) fall, and (d) winter. Units are $\mu\text{g m}^{-3}$.

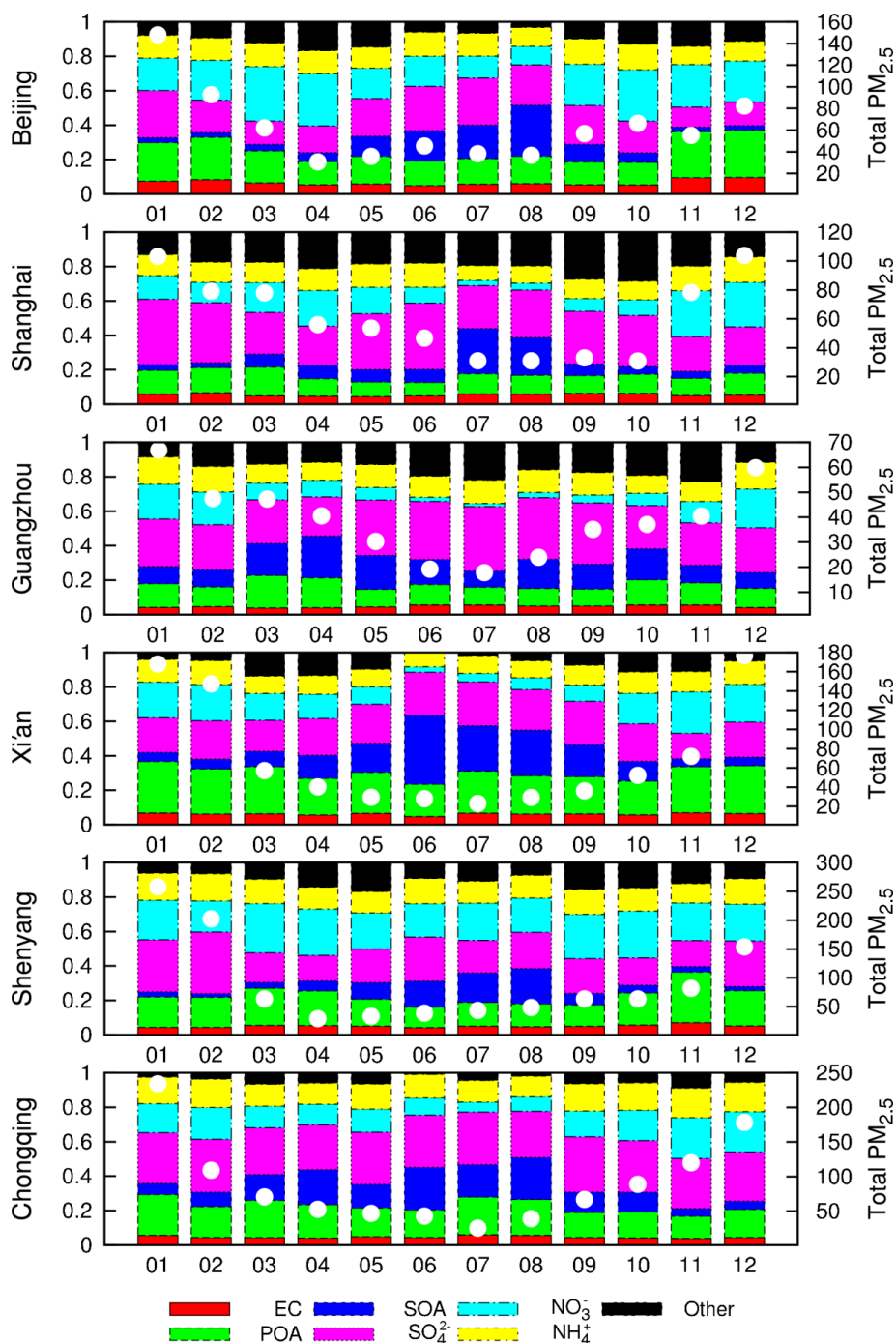


706
707

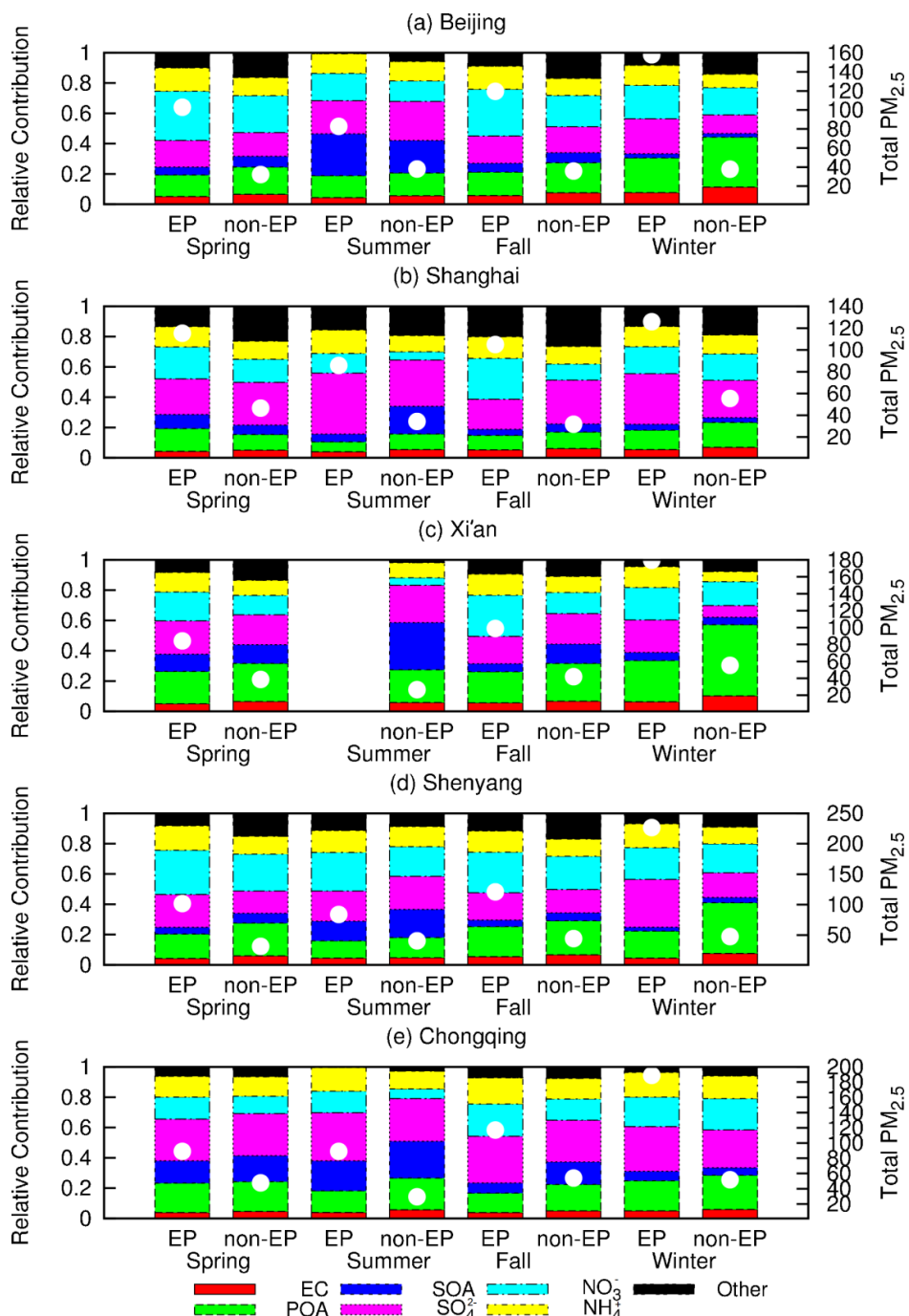
Figure 7. Seasonal variations of predicted $PM_{2.5}$ components. Units are $\mu g m^{-3}$.



708
709 Figure 8 Deviation of winter nitrate (NO_3^-), sulfate (SO_4^{2-}), ammonium ion (NH_4^+) and primary
710 organic aerosol (POA) from annual average, as calculated by $(W-A)/A$, where W and A are win-
711 ter and annual concentrations, respectively.
712



713
 714 Figure 9. Contributions of different components to monthly averaged $PM_{2.5}$ concentrations at
 715 selected cities in China. White circles are absolute concentrations according to right y-axis with
 716 unit of $\mu g m^{-3}$.



717
 718 Figure 10. Comparison of PM_{2.5} components at episode days (EP, $\geq 75 \mu\text{g m}^{-3}$) and non-episode
 719 days (non-EP, $< 75 \mu\text{g m}^{-3}$). White circles are absolute concentrations according to right y-axis
 720 with unit of $\mu\text{g m}^{-3}$. Note Xi'an does not have episode days in summer.